J.F.B.D. Fonseca[1], M. Palano[2], A.P. Falcão[3], A. Hrysiewicz[4], and J. Fernández[5]

[1] CERENA, Instituto Superior Técnico, Universidade de Lisboa, Av Rovisco Pais 1, 1049-001 Lisboa, Portugal.

[2] Istituto Nazionale di Geofisica e Vulcanologia, Osservatorio Etneo - Sezone di Catania, Piazza Roma 2, 95125 Catania, Italy.

[3] CERIS, Instituto Superior Técnico, Universidade de Lisboa, Av Rovisco Pais 1, 1049-001 Lisboa, Portugal.

[4] UCD School of Earth Sciences, University College Dublin, Dublin 4, Ireland.

[5] Institute of Geosciences (CSIC-UCM), C/ Doctor Severo Ochoa, 7, Ciudad Universitaria, 28040-Madrid, Spain.

Corresponding author: João F.B.D. Fonseca (`jfonseca@tecnico.ulisboa.pt`)

Key Points:

- We present a GNSS velocity for the southern Lusitanian Basin and Lower Tagus and Sado Basin
- We complement those results with PSInSAR-derived vertical velocities for the Lisbon Metropolitan Area
- The area in under sinistral simple shear, with velocities and strain-rates pointing to higher seismic hazard than previously estimated.

Abstract

The Lisbon Metropolitan Area (LMA, Portugal) has been affected by several destructive earthquakes nucleating both along the offshore Africa-Eurasia plate boundary and on onshore inherited intraplate faults. Using a dense GNSS dataset coupled with PSInSAR analysis, we provide new evidence of sinistral simple shear driven by a NNE-SSW first-order tectonic lineament. PSInSAR vertical velocities corroborate the GNSS strain-rate field, showing uplift/subsidence where the GNSS data indicate contraction/extension. We suggest the presence of a small block to the W of Lisbon moving independently towards the SW with a relative velocity of 0.96±0.20 mm/yr, whose boundaries are part of a complex and as yet poorly constrained strike-slip fault system, possibly rooting at depth into a simpler basement fault. Comparison between geodetic and seismic moment-rates indicates a high seismic coupling. We show that the contribution of intraplate faults to the seismic hazard in the LMA may be more important than currently assumed.

Plain Language Summary

Space geodesy (using the Global Navigation Satellite System or RADAR images obtained by satellites) allows for the detection and characterization of surface deformation when points at the Earth's surface move with velocities of the order of 1 mm per year or higher. Using 15-year long series of GNSS observations and 6-year long series of RADAR images from ESA's Sentinel-1 satellites, we

characterize the deformation of the Lisbon Metropolitan Area. We conclude that the crust is being stretched in NE-SW direction, and on top of this pattern we detect a local patch of contraction, near the Tagus river bar. Because the deformation occurs on a sedimentary basin, we have to infer indirectly the type of deformation that takes place in the underlying basement, where the earthquakes nucleate. We conclude that two blocks of crust are sliding horizontally past each other along the Lower Tagus Valley, inducing a style of deformation in the sediment cover called simple shear, while a smaller block between Lisbon and Cascais moves independently with respect to its surroundings. Our results indicate that the faults near Lisbon probably contribute more to the seismic hazard of the region then assumed in previous studies, with implications for the building regulations.

1 Introduction

The southern sector of the Lusitanian basin, SW Portugal (Figure 1a), has been the locus of relevant seismicity in historical time (Moreira, 1985; Stucchi et al., 2013). The list of known destructive earthquakes affecting the region and the adjacent continental shelf ranges in time from 1344 to 1909, with catastrophic occurrences in 1356, 1531 and 1755 (https://www.emidius.eu/SHEEC). Because of the tsunamigenic nature of the 1755 earthquake, the existence of important seismogenic structures offshore SW Portugal was recognized at an early stage. The 1909 earthquake, however, with epicenter ~40 km to the NE of Lisbon and estimated magnitude in the range M6.0-M6.5, had a clear intraplate nature, and it is widely accepted that the M7 1531 earthquake also nucleated onshore, in the active structures of the Lower Tagus Valley (Justo and Salwa, 1998; Canora et al., 2020). All these features point toward a diffuse zone of deformation involving both onshore and offshore active structures which accommodate the Nubia-Eurasia plate convergence through a relevant seismicity release, as recently proposed by Palano et al. (2015). The relative importance of the contributions of onshore versus offshore seismic sources to seismic hazard in Portugal is largely debated. On one hand, in view of the modest convergence rate (~4 mm/year in a NW-SE direction; Fernandes et al., 2003), it has been argued that most of the cumulated crustal deformation is fully released by 1969-type offshore earthquakes of the Gulf of Cadiz, implying that intraplate faults account for very small slip-rates. It follows that destructive intraplate earthquakes are deemed very rare events with limited contribution to the probabilistic hazard (e.g., Ramalho et al. 2020). This view is supported by very low intraplate slip-rate estimates derived from geological studies (0.005 to 0.3-0.5 mm/yr; Cabral, 2012). On the other hand, seismic hazard disaggregation studies have led to opposite conclusions, whereby the rupture of a nearby intraplate fault is the dominant scenario contributing to the hazard in the vicinity of Lisbon (Vilanova and Fonseca, 2007; Woessner et al., 2015).

Space geodesy may hold the key to arbitrate this issue, since in conjunction with instrumental seismicity it allows the direct observation and quantification of interseismic strain buildup (Bennet et al., 1998; Murray et al., 2014; Lange et

al., 2019). The southern Lusitanian basin hosts a significant number of GNSS stations at an average spacing of ~30 km, continuously operating in the last 15 years. To constrain both intraplate deformation style and rates of the southern sector of the Lusitanian basin we used the available GNSS data. In addition, PSInSAR analysis was used to provide further constraints on the vertical component of motion, with increased spatial resolution and similar precision.

2 Regional tectonics

The Lisbon Metropolitan Area (LMA; Figure 1a) is located on the southern sector of the Lusitanian Basin (LB) in the western coast of Iberia, a magma-poor rift margin that formed ~200 million years ago, when the North Atlantic rift system incised the Paleozoic crust of the Hesperic Massif in the Late Triassic (Wilson, 1989; Rasmussen et al., 1998). At the early stages of passive margin evolution, the LB formation was controlled by a set of crustal-scale strike-slip faults (Aveiro fault, Nazaré fault, Lower Tagus Valley fault, Messejana-Ávila fault) inherited from the Hercynian Orogeny (Arthaud and Matte, 1977; Pinheiro et al., 1996; Pereira and Alves, 2013). The study area straddles one of the hypothesised Hercynian crustal fractures, the Lower Tagus Valley fault (LTVF). Triassic and Early Jurassic deposits comprise important amounts of evaporites, the Dagorda formation, which accumulated in grabens and half-grabens at depths raging from 2 km to 4.5 km and thicknesses from 200 m to 1500 m (Rasmussen et al., 1998; Reis et al., 2017). With the onset of seafloor spreading in the Mid Jurassic, the rifting axis shifted to the west and the LB became an aborted rift (Hubbard, 1988). A new set of extensional faults developed at this stage to accommodate the subsidence of the margin (Montenat et al., 1988), and halokinesis played an important role in the evolution of the LB, with different sectors developing independently as fault-bounded or salt-wall bounded sub-basins (Alves et al., 2003). The main faults through the sediment fill of the LB revelaled by commercial seismic reflection data (Walker, 1982) are depicted in Figure 1a. During the Alpine Orogeny the LB underwent structural inversion (Curtis, 1999), which stops abruptly at the ENE-WSW Arrabida range, the southern limit of the LB (A. Fonseca et al., 2020). Palaeoseismological and geomorphological investigations have unveiled evidence of Holocene rupture on two parallel strands of faults along the margins of the Tagus River (Figure 1a) with geomorphic indicators of sinistral strike-slip (Ostman et al., 2012, Canora et al., 2015; Canora et al, 2021), in response to the LTVF reactivation by the current stress field, characterized by a NW-SE maximum compressive stress (Ribeiro et al., 1996). The southern sector of the LB hosts significant historical seismicity (Moreira, 1989; Stucchi et al., 2012), but during the last decades the region has experienced quiescence (Custodio et al., 2015), with only M<3 earthquakes that form a diffuse pattern (Figure 1b).

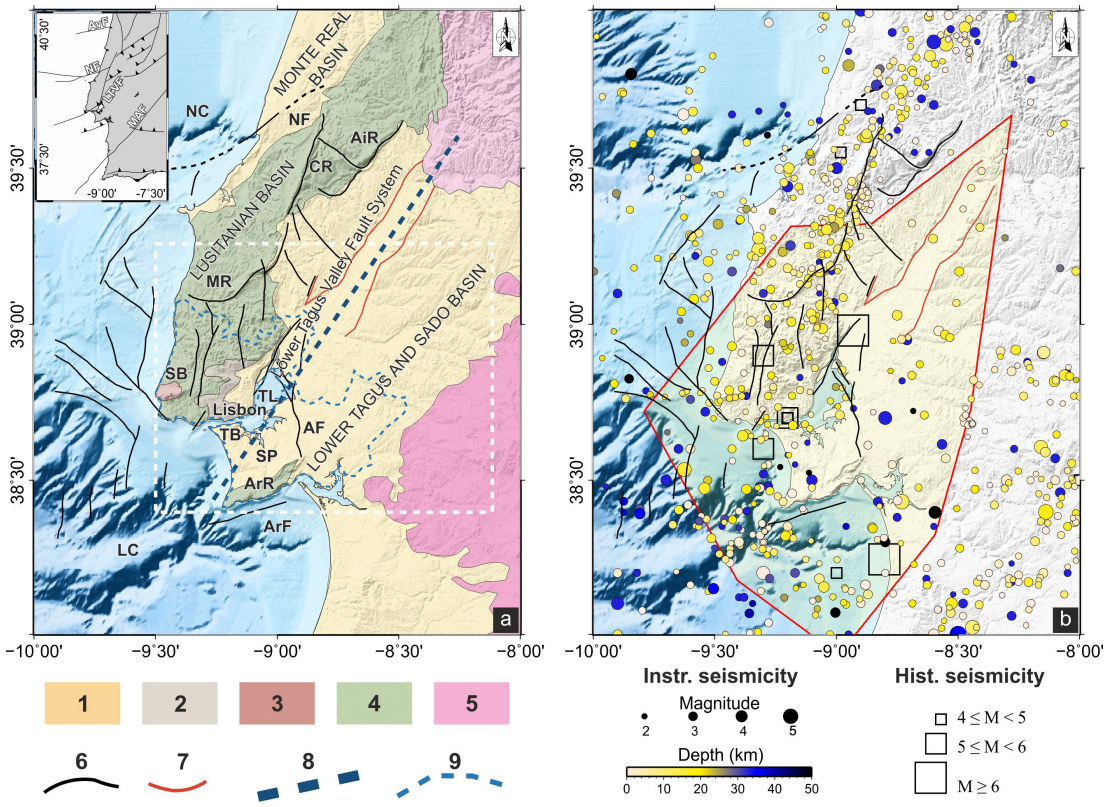

Figure 1. a) Simplified geology of the Lusitanian Basin and adjacent Cenozoic basins, after the 1:10000 Geological Map of Portugal (LNEG, 2010). Faults (black lines) after Walker (1982), Dickson (1992) and Curtis (1999). Holocene ruptures (red lines) after Canora et al. (2020). The dashed white rectangle delimits the study area. Number in legend are: 1) Cenozoic sediments, 2) Lisbon Volcanic Complex, 3) Sintra batholith, 4) Mesozoic sediments, 5) Paleozoic basement, 6) generic fault, 7) fault with Holocene activity, 8) inferred basement fault (Lower Tagus Valley Fault), 9) limits of the Lisbon Metropolitan Area. Abbreviations are: AvF, Aveiro fault; NF, Nazaré fault; LTVF, Lower Tagus Valley fault; MAF, Messejana-Ávila fault; AF, Alcochete fault; AiR, Aire Range; NC, Nazaré Canyon; CR, Candeerios Range; MR, Montejunto Range; SB, Sintra batholith; TL, Tagus lagoon; TB, Tagus bar; SP, Setúbal Peninsula, ArR, Arrábida Range; ArF, Arrábida fault. b) Seismicity of study area and surrounding region. Instrumental seismicity (1964-2020) from the International Seismological Center (http://www.isc.ac.uk). Historical seismicity after the SHEEC catalog (Stucchi et al., 2013). The yellow polygon represents the area used for moment rate comparisons.

3 Data and methods

All available GNSS continuous stations covering the study area were processed

using the GAMIT/GLOBK 10.71 software (Herring et al. 2018; http://www-gpsg.mit.edu), adopting the strategy described in the Supplementary Information. To improve the overall configuration of the network and tie the regional measurements to an external global reference frame, data coming from more than 100 continuously operating global tracking stations were also introduced in the processing (Figure S1). To adequately show the crustal deformation pattern over the investigated area, the GNSS velocity field has been aligned to a fixed Eurasian reference frame (Altamimi et al., 2017). The resulting velocity field, with error ellipses at the 95 percent confidence level, is shown in Figure 2a).

Vertical velocities were also computed using 311 ascending-orbit (306 descending-orbit) Sentinel-1 Synthetic Aperture Radar images (Burgmann et al., 2000) acquired between 2014 and 2020, with the PSInSAR ((Persistent Scatterer Interferometric SAR) technique (Ferretti et al., 2000), using the GAMMA software (Werner et al., 2000; Wegmuller et al., 2019). These results are independent from the GNSS vertical velocity estimates and have a much higher spatial resolution. Figure 3 displays the estimated vertical velocities, and the reference points. See the Supplementary Information for additional details.

4 Results

The horizontal velocities with respect to stable Eurasia for 20 GNSS stations on the LB and on the adjacent LTSB are reported in Figure 2a. In general, the stations move towards the NW quadrant with an average velocity of ~1.5 mm/yr. We selected for further analysis a subset of 12 stations located on the LMA (see the red dashed rectangle in Figure 2a). In order to filter out short-wavelength deformations while retaining the regional pattern, we compared each horizontal velocity with the average of the four nearest sites. It can be seen (Figure 2b) that IGEO station deviates significantly from the neighbor stations, which might be due to monument instability or localized deformation of geotechnical origin. For this reason, the IGEO station will be excluded from the analysis of the regional deformation. To the W of the Tagus estuary, a few other sites show significant deviations, but in a coherent pattern. The average velocity of the three stations with green arrows with respect to the average velocity of the remaining eight sites of the study area (red dashed rectangle) is *0.96±0.20 mm/yr*, with an azimuth of ~217^{o} (red arrow in figure 2a). The velocity of station CASC is different from those immediately to its E, but not dissimilar from the average velocity of the region. Because station CASC has a robust monument and a long history of observation (1997 to present) we accept its velocity as a reliable result. The significance of these anomalous velocities will be discussed below.

Using the 11 sites retained in the analysis, we considered as baselines all the 55 segments connecting any two sites, and for each baseline we computed its shortening/extension and its rotation. In the following description, point 1 is always the westernmost end of the segment, and point 2 is the easternmost end. Representing by r_{12} the length of the baseline, by $\hat{u}_{12}$ the unit vector directed from point 1 to point 2, and by $\vec{v}_{12}$ the relative velocity of point 1 with respect

to point 2, we measured the rate of shortening of each baseline by

$v_{//} = \vec{v}_{12}.\ \hat{u}_{12}$,

and its rate of rotation by

$$\omega = \frac{v_{\perp}}{r_{12}}$$

with

$$v_{\perp} = \sqrt{|\vec{v}_{12}|^2 - {v_{//}}^2}$$

Figures 2c and 2d show the results for all the 55 baselines. The angle in the horizontal axis is the azimuth of the baseline with respect to North (positive clockwise). Positive values of $v_{//}$ correspond to shortening, and positive values of ω correspond to counterclockwise rotation.

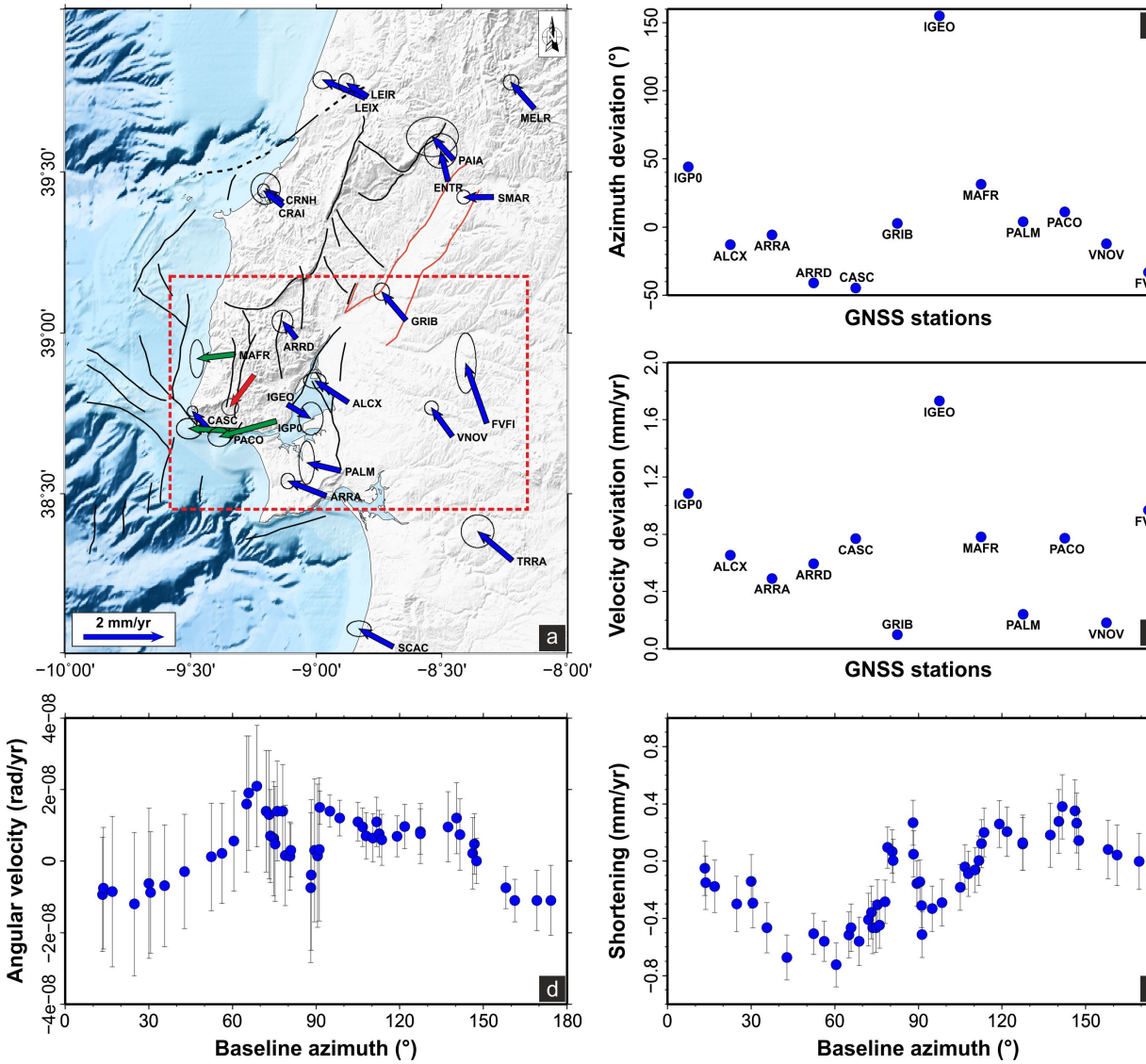

Figure 2. a) GNSS-derived velocity field with respect to stable Eurasia. The ellipses represent 95% confidence intervals. Stations located in the red dashed rectangle have been analyzed to filter out short-wavelength deformations (see the main text for details). The red arrow is the average velocity of the three sites colored in green relative to the average velocity at the remaining stations. b) Deviation of the azimuth of velocity of each site with respect to the average velocity of the four nearest sites. c) Deviation of the scalar velocity of each site with respect to the average of the four nearest sites. d) Baseline rotation as a function of azimuth. Positive angular velocities correspond to counterclockwise rotation. e) Baseline shortening/extension as a function of azimuth. Positive

values correspond to shortening. Azimuths are reckoned clockwise from North.

Figure 3 shows the vertical velocities inferred from the PSInSAR analysis using ascending and descending orbits, ranging from *3 mm/yr* of subsidence to *1 mm/yr* of uplift (in the same reference frame adopted for the GNSS-derived velocities). Subsidence is dominant near the margins of the Tagus river and on the eastern side of the Setubal peninsula, displaying a close association with the faults that cut through the post-Oligocene sediments of the LTSB (black lines in Figure 3). A zone of uplift can be observed to the immediate W of the city of Lisbon straddling the Tagus bar, with a NNE-SSW trend. Other patches of uplift can be seen further to the SE in the Setubal peninsula and further to the NW. A narrow band of subsidence can be observed to the North of, and parallel to, the uplifting Arrábida range.

Finally, Figure 4 depicts the horizontal strain-rates estimated on a regular 0.1° x 0.1° grid over the investigated area by adopting the method reported in Shen et al. (2015). See Supplementary Material for details. The resulting strain-rate field is characterized by a sharp extension of ~15 nstrain/yr with axis NE-SW coupled with a small contraction (3-4 nstrain/yr) along the NW-SE extension. A local patch of contraction also ~15 nstrain/yr can be observed close to the Lisbon -Tagus bar area with the shortening axis oriented NNE-SSW.

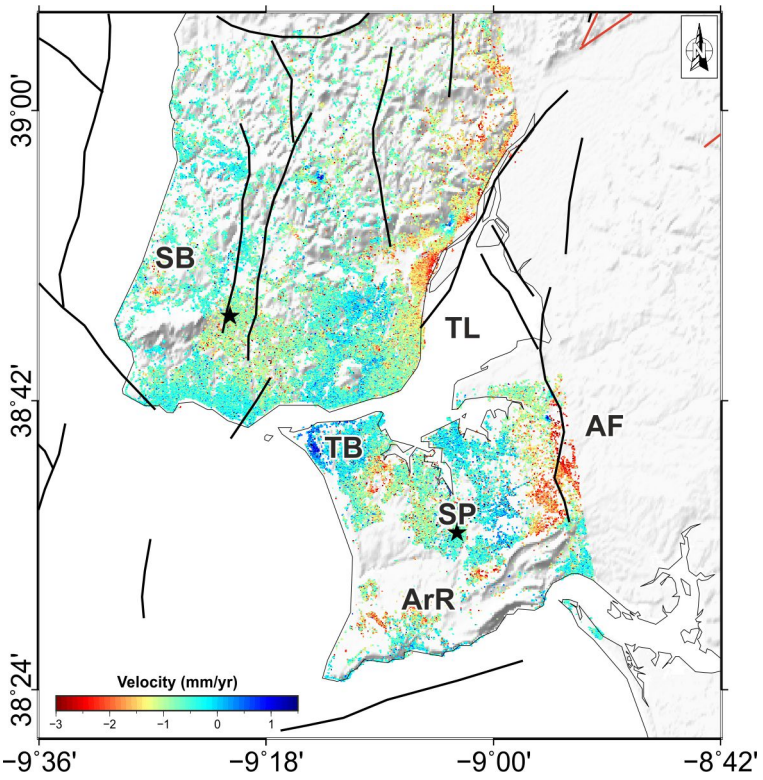

Figure 3. Permanent Scatterer InSAR vertical velocities in the study area (531798 points), derived from Sentinel-1 images (311 ascending and 306 descending orbits) acquired by ESA between 2014 and 2020. Positive velocities (cold colors) correspond to uplift, negative velocities (warm colors) correspond to subsidence. The velocities were computed adopting two reference points, shown in the figure as black stars, and then converted to the GNSS velocity reference frame (see text for details). The black lines depict faults through the sediment cover. Abbreviations are as Figure 1.

5 Discussion

5.1 Active tectonics of the LMA

A first-order observation, according to the geodetic strain-rate field (Figure 4a), is that the crust of the LMA is esperiencing NE-SW extension, except in the zone around the Tagus bar which displays significant NNE-SSW shortening. This is consistent with the PSInSAR estimates of vertical velocity (Figure 3), showing uplift near the Tagus bar but mostly subsidence elsewhere. This extensional regime is also consistent with the evolution of the Tagus lagoon, the only zone of Portugal to display subsidence during the Quaternary (Cabral, 2012).

Figures 2d and 2e provide further insight into the horizontal deformation pattern. Baselines having the azimuth in the range N30E to N110E undergo predominantly extension (Figure 2d), in agreement with the strain-rate map (Figure 4a). Baselines with azimuth in the range N70W to N20W display shortening instead, also consistent with the strain-rate field. Moreover, Figure 2d shows that most baselines rotate counterclockwise, with a few exceptions in the range N30W-N50E. Taken together, these results are strongly indicative of simple sinistral shear above a strike-slip fault with NNE-SSW orientation, as depicted schematically in Figure 4b. Segments connecting stations with green arrows in Figure 2 tend to show anomalous behavior, visible near azimuth N85E, showing contraction and rotating clockwise against the dominant tendency. Together with the observation that this group of sites moves with an average velocity of 0.97 ± 0.20 *mm/yr* towards the SW quadrant with respect to the average velocity of the remaining sites, this behavior indicates the presence of a small crustal block to the W of Lisbon, moving independently, possibly related to a local lateral extrusion process. The eastern boundary of this block may be tentatively associated with the transition from uplift to subsidence (Figure 3) along a line that runs between sites IGP0 and IGEO (Figure 2). On the western side, it can be speculated that CASC is "pinned" by the Sintra batholith that lays to its north. Paleoseismological and geomorphological investigations are probably the only path to improve our understanding of the active deformation of the region, despite the challenges put by the urban development of the LMA.

A likely explanation for the complex pattern of deformation near Lisbon concerns the connection of the LTVF with the offshore fault system (Figure 1a). As it approaches the broad lagoon of the Tagus estuary, the fault system swings to a N-S direction along the Alcochete fault, in a releasing bend (e.g., Sylvester,

1988) that causes NE-SW extension and subsidence. Figure 3 shows that this subsidence is linked to the activity of the fault system, confirming that the Tagus lagoon is an active pull-apart basin as proposed by Vilanova and Fonseca (2004). When it reaches the S of the Arrabida range, the fault system changes direction again, adopting a ENE-WSW strike and dip-slip motion (Figure 4b), changes of direction and style that configure a single restraining bend (Cunningham and Mann, 2007), explaining the compression and uplift detected in the Setúbal Peninsula.

Our results do not clarify to what extent this complexity is also present at basement level, given the effective detachment at the base of the sediment fill ((Rasmussen et al, 1998; Reis et al., 2017).The uplift observed south of the Tagus bar (Figure 3) is aligned with the trend of the LTVF further to the NE, and this may indicate that at depth the crustal fault continues as a linear feature towards the offshore. Although the tectonic relevance of the canyons has been a topic of speculation for many decades (Pinheiro et al, 1996; Pereira and Alves, 2013), it is a fact that they are aligned with major crustal faults (see inset in Figure 1a) further north (Nazaré fault) as well as further South (Messejana-Ávila fault). A continuation of the linear trend described above through the continental shelf is therefore supported by its alignment with the Lisbon Canyon (Lastras et al., 2009).

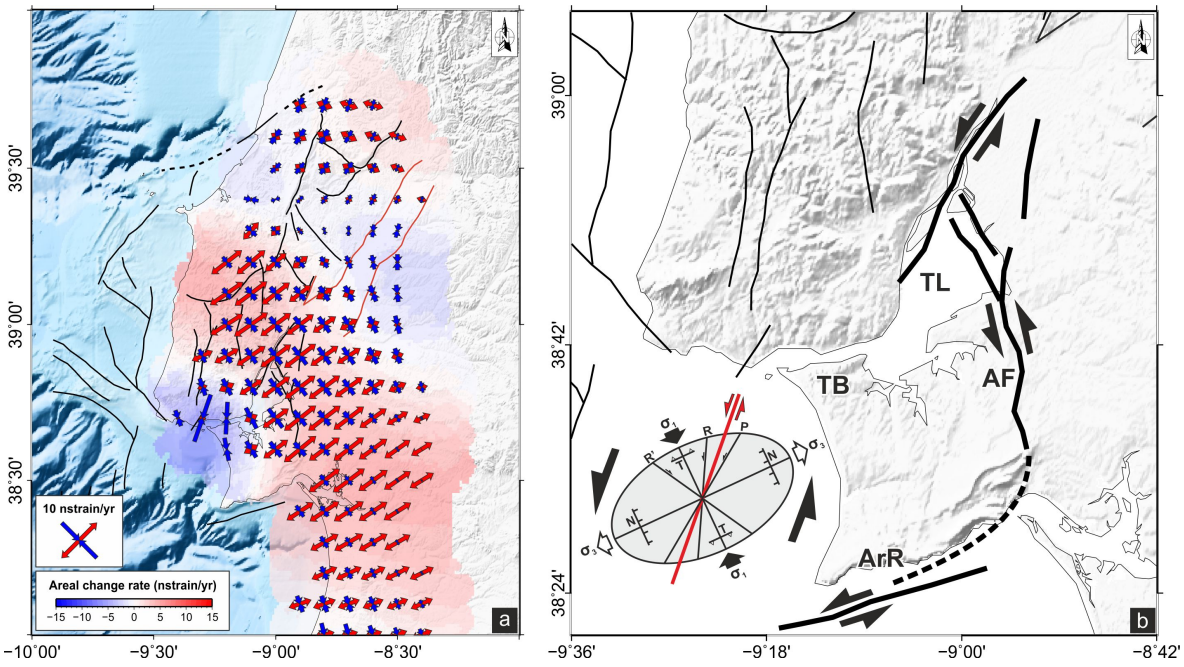

Figure 4. a) Strain-rates inferred from the GNSS horizontal velocities (see text for details). Blue corresponds to areas under compression, pink to areas under extension. b) Schematic tectonic interpretation of the study area. Abbrevia-

tions are: AF, Alcochete fault; ArR, Arrábida Range; TL, Tagus lagoon; TB, Tagus bar. Inset: schematic representation of the simple-shear deformation of ductile sediment cover on top of a sinistral strike slip fault. Red line: underlying basement fault; R, synthetic Riedel shear; R', antithetic Riedel shear; N, normal fault, T, thrust and reverse fault; P, secondary synthetic shear; $_1$ and $_3$, principal stress axes. Modified from Sylvester (1988).

5.2 Moment rate estimates

Geodetically-derived strain cannot be equated directly to seismic moment release, since a significant percentage of the deformation may be aseismic (e.g., Masson et al., 2005; Palano et al., 2018). Taking as reference the source area used by Woessner et al. (2015) to account for the seismicity of the Lower Tagus Valley (depicted in Figure 1b), and using *15 km* for seismogenic thickness and *30 GPa* for crustal rigidity, we estimate a value of $\dot{M}_0^{\text{geod}} = 1.35x10^{17} Nm/yr$ for the scalar geodetic moment-rate (see how in the Supplementary Information). Ramalho et al. (2020) reviewed the probabilistic seismic hazard assessment of Woessner et al. (2015) and estimated $\dot{M}_0^{\text{seis}}$ from the Gutenberg-Richter parameters for the same source area for which we estimated $\dot{M}_0^{\text{geod}}$, so a direct comparison between the two results can be performed. For the three values of maximum magnitude (7.1, 7.4 and 7.6) considered by Woessner et al. (2015), Ramalho et al. (2020) obtained $\dot{M}_0^{\text{seis}}$ of 8.69x10^{16} Nm/yr, 1.33 x10^{17} Nm/yr and 1.77 x10^{17} Nm/yr, respectively. These values compare well with our geodetic estimate of the moment-rate, especially the central value, suggesting a strong seismic coupling of the area.

Finally, it is important to confront assumptions regarding seismic hazard with the new results put forward here. Cabral et al. (2012) state that the intraplate faults of Western Iberia have very slow slip-rates, in the range 0.005 to 03-0.5 mm/yr, with return periods larger than 5000 years for M>6 earthquakes, having therefore a small contribution to the hazard at the regulatory return period of 475 years when compared to more distant offshore faults. Our results suggest that these values are exceeded in the vicinity of Lisbon. Although the velocities and rates reported here cannot be directly extrapolated to the basement given the likely detachment at the bottom of the basin fill, it can be stated that the observed strain-rates, of the order of *15 nstrain/yr* or *~5x10^{-16} s^{-1}*, are higher than those typically associated with intraplate areas (*10^{-17}* to *10^{-20} s^{-1}* according to Molnar, 2020) and are comparable to those observed in the Basin and Range (*~3x10^{-16} s^{-1}* according to Payne et al., 2008) or in Southern Tibet *(~4x10^{-16} s^{-1}* according to Wang et al., 2019).

5 Conclusive remarks

The analysis of GNSS data in the LMA revealed a pattern of interseismic deformation consistent with simple shear on top of a locked strike slip basement fault oriented NNE-SSW, with strain-rates of the order of *15 nstrain/yr*, both extensional and contractional. Vertical velocities independently derived from radar images with the PSInSAR technique broadly corroborate these results, show-

ing uplift (subsidence) where the GNSS data detect contraction (extension). A block to the West of Lisbon, sampled by three GNSS sites, moves with respect to the surrounding region on both sides with a relative velocity of 0.96±0.20 mm/yr, possibly as the result of small-scale lateral extrusion. These results support the hypothesis that the Lower Tagus Valley is the locus of an active first-order crustal fault which drives the observed simple shear surface deformation, while contradicting the widespread view (e.g., Ramalho, 2020) that the LTV faults are too slow to contribute with a major parcel of the seismic hazard of the region. The impact of intraplate faults in the seismic hazard in the LMA may therefore be more important than currently assumed, among other studies, by the EUROCODE 8 National Document for Portugal (Costa et al., 2008).

Acknowledgments

J.F.B.D.F. acknowledges support from the Portuguese research foundation FCT, under Line of Excellence grant EXCL/GEO-FIQ/0411/2012 - Seismicity of Plate Interiors: Challenges to Hazard Evaluation. A.P.F. acknowledges support from AGEO - Platform for Atlantic Geohazard Risk Management (https://ageoatlantic.eu/, grant no. EAPA_884/2018. A.H. thanks the European Space Agency (ESA) for providing the Sentinel-1 IW SAR data, NASA for offering the SRTM DEM via the Earth Explorer website (https://earthexplorer.usgs.gov) and GAMMA's staff for InSAR support. Research by M.P. and J.F. was supported by the AEI Spanish research project DEEP-MAPS, grant agreement number RTI2018-093874-B-100. This work represents a contribution to CSIC Thematic Interdisciplinary Platform PTI TELEDETECT. The RINEX data of the SERVIR CORS and ReNEP networks used in this paper were kindly yielded by the Instituto Geográfico do Exército, Lisbon (www.igeoe.pt) and Direcção Geral do Território, Lisbon (https://renep.dgterritorio.gov.pt/), respectively. Access is subject to a "data use agreement", and interested scientific users (universities, research rnstitutes, governmental ecientific agencies, etc.) can obtain free access by contacting these entities. Instrumental seismicity data were downloaded from the International Seismological Centre website http://www.isc.ac.uk (Storchak et al., 2020). Sentinel-1 IW SAR data was downloaded from ESA's Copernicus hub https://scihub.copernicus.eu/. All figures were prepared with the GMT software (Wessel and Smith, 1991).

References

Altamimi, Z., P. Rebischung, L. Métivier, & X. Collilieux (2016), ITRF2014: A new release of the International Terrestrial Reference Frame modeling nonlinear station motions. *J. Geophys. Res. Solid Earth*, 121, 6109–6131, doi:10.1002/2016JB013098.

Alves, T.M., Gawthorpe, R.L., Hunt, D.W. , & Monteiro, J.H. (2003), Cenozoic tectonosedimentary evolution of the western Iberian margin. *Marine Geology*, 195, 75–108. http://dx.doi.org/10.1016/S0025-3227(02)00683-7.

Arthaud, F. , & Matte, P. (1977), Late palaeozoic strike-slip faulting in southern Europe and Northern Africa: Result of a right-lateral shear zone between the

Appalachians and the Urals. *Geol. Soc. Am. Bull.*, 88, 1305–1320.

Bekaert, D.P.S., Walters, R.J., Wright, T.J., Hooper, A.J. , & Parker, D.J. (2015), Statistical comparison of InSAR tropospheric correction techniques. *Remote Sensing of Environment,* 170, 40–47.

Bennett, R.A., Wernicke, B.P., & Davis, J.L. (1998), Continuous GPS measurements of contemporary deformation across the northern Basin and Range province. *Geophysical Research Letters*, 25(4), 563-566.

Boehm, J., B. Werl, & H. Schuh (2006), Troposphere mapping functions for GPS and very long baseline interferometry from European Centre for Medium-Range Weather Forecasts operational analysis data. *J. Geophys. Res. Solid Earth*, 111, B02406, doi:10.1029/2005JB003629.

Burgmann, R., Rosen, P. A., & Fielding, E. J. (2000), Synthetic aperture radar interferometry to measure Earth's surface topography and its deformation. *Annual Review of Earth and Planetary Sciences*, 28, 169–209.

Cabral, J. (2012), Neotectonics of mainland Portugal: state of the art and future perspectives. *Journal of Iberian Geology*, 38(1), 71-84, 2012.

Cabral, J. , & Ribeiro, A. (1988), Carta Neotectónica de Portugal Continental, Serviços Geológicos de Portugal, Lisbon (in Portuguese).

Canora, C., S.P. Vilanova, G.M.B. Ostman, J. Carvalho, S. Heleno, & J.F.B.D. Fonseca (2015), The Eastern Lower Tagus Valley Fault Zone in central Portugal: Active faulting in a low-deformation region within a major river environment. *Tectonophysics*, 660, 117–131. doi:10.1016/j.tecto.2015.08.026

Canora C, Vilanova SP, De Pro-Diáz Y, Pina P., & Heleno, S. (2021), Evidence of Surface Rupture Associated With Historical Earthquakes in the Lower Tagus Valley, Portugal. Implications for Seismic Hazard in the Greater Lisbon Area. *Front. Earth Sci.*, 9, 620778. doi: 10.3389/feart.2021.6

Costa, A. C., Sousa, M. L., & Carvalho, A. (2008), Seismic zonation for Portuguese national annex of Eurocode 8. In *Proceedings of the 14th World Conference on Earthquake Engineering*, China, 2008.

Crosetto, M., Monserrat, O., Cuevas-González, M., Devanthéry, N. , & Crippa, B. (2016), Persistent Scatterer Interferometry: A review. *ISPRS Journal of Photogrammetry and Remote Sensing*, 115, pp. 78-89, https://doi.org/10.1016/j.isprsjprs.2015.10.011.620778

Cunningham, W.D. , & Mann, P (2007), Tectonics of strike-slip restraining and releasing bends. In Cunningham, W.D. and Mann, P. (eds), Tectonics of Strike-Slip Restraining and Releasing Bends, Geological Society, London, Special Publications, 290, 1–12.

Curtis, M.L. (1999), Structural and kinematic evolution of a Miocene to Recent sinistral restraining bend: The Montejunto massif, Portugal. *J. Struct. Geol.*, 21, 39–54.

Custódio, S., N. A. Dias, F. Carrilho, E. Góngora, I. Rio, C. Marreiros, I. Morais, P. Alves, , & L. Matias (2015), Earthquakes in Western Iberia: Improving the understanding of lithospheric deformation in a slowly deforming region. *Geophys. J. Int.,* 203, 127–145.

Dickson, A.J. (1992), A Regional Seismic Interpretation of Offshore Portugal. M.Sc. Thesis, University of Durham, U.K.

Fernandes, R. M. S., Ambrosius, B. A. C., Noomen, R., Bastos, L., Wortel, M. J. R., Spakman, W., & Govers, R. (2003), The relative motion between Africa and Eurasia as derived from ITRF2000 and GPS data. *Geophys. Res. Lett.*, 30, 1828–1840.

Ferretti, A., Prati, C., & Rocca, F. (2000), Non-linear subsidence rate estimation using persistent scatterers in differential SAR interferometry. *IEEE Transactions on Geoscience and Remote Sensing*, 38(5), pp. 2202–2212.

Fonseca, A.F., Zêzere, J.L. , & Neves, M. (2020), The Arrabida Chain: the Alpine Orogeny in the vicvinity of the Atlantic Ocean. In G. Vieira et al. (eds.), Landscapes and Landforms of Portugal, World Geomorphological Landscapes, Springer Nature, https://doi.org/10.1007/978-3-319-03641-0_21

Fujiwara, S., Nishimura, T., Murakami, M., Nakagawa, H., Tobita, M. , & Rosen, A.P. (2000), 2.5-D surface deformation of M6.1 earthquake near Mt Iwate detected by SAR interferometry. *Geophysical Research Letters*, 70 (14), 2049-2052.

Herring, T.A. (2003), MATLAB Tools for viewing GPS velocities and time series. *GPS Solutions*, 7582 (3), 194-199, doi:10.1007/s10291-003-0068-0. 583

Herring, T.A., King, R.W., Floyd, M.A. , & McClusky, S.C., (2018), Introduction to GAMIT/GLOBK, Release 10.7. Massachusetts Institute of Technology: Cambridge, UK.

Hubbard, R.J. (1988), Age and significance of sequence boundaries on Jurassic and early Cretaceous rifted continental margins. *Am. Assoc. Petr. Geol. Bull.*, 72 (1), 49–72.

Justo, J. L. , & C. Salwa (1998), The 1531 Lisbon Earthquake. *Bull. Seism. Soc. Am.*, 88 (2), 319–328.

Lange, D., Kopp, H., Royer, J.-Y., Henry, P., Çakir, Z., Petersen, F., Sakic, P., Ballu, V., Bialas, J., Özeren, M.S., Ergintav, S. , & Géli, L. (2019), Interseismic strain build-up on the submarine

North Anatolian Fault offshore Istanbul. *Nature Communications*, 10:3006, https://doi.org/10.1038/s41467-019-11016-z

Lastras, G., Arzola, R.G., Masson, D.G., Wynn, R.B., Huvenne, V.A.I., Huhnerbach, V., & Canals, M. (2009), Geomorphology and sedimentary features in the Central Portuguese submarine canyons, western Iberian margin. *Geomorphology*, 103(3), 310-329, doi: 10.1016/j.geomorph.2008.06.013

Lyard, F., Lefevre, F., Letellier, T., & Francis, O. (2006), Modelling the global ocean tides: Modern insights from fes2004. *Ocean Dyn.*, 56, 394–415

Masson, F., Chery, J., Hatzfeld, D, Martinod, J., Vernant, P., Tavakoli, F., & Ghafory-Ashtiani, M. (2005), Seismic versus aseismic deformation in Iran inferred
from earthquakes and geodetic data. *Geophys. J. Int.*, 160, 217—226, doi: 10.1111/j.1365-246X.2004.02465.x

Molnar, P. (2020), The brittle-plastic transition, earthquakes, temperatures, and strain-rates. *Journal of Geophysical Research: Solid Earth*, 125, e2019JB019335. https://doi.org/ 10.1029/2019JB019335

Montenat, C., Guery, F., Jamet, M. , & Berthou, Y.B. (1988), Mesozoic evolution of the Lusitanian Basin: comparison with the adjacent margin. In Boillot, G., Winterer, E.L., et al., Proc. ODP, Sci. Results, 103: College Station, TX (Ocean Drilling Program), pp. 757-775.

Moreira, V. (1989), Seismicity of the Portuguese continental margin. In S. Gregersen and P. Basham (Editors), Earthquakes at North-Atlantic Passive Margins: Neotectonics and Postglacial Rebound, Kluwer Academic Publishers, 533–545.

Murray, J. R., Minson, S. E. , & Svarc, J. L. (2014), Slip rates and spatially variable creep on faults of the northern San Andreas system inferred through Bayesian inversion of Global Positioning System data. *J. Geophys. Res. Solid Earth*, 119,6023–6047,doi:10.1002/2014JB010966.

Ostman, G.M.B., S.P. Vilanova, E.S. Nemser, A. Falcao-Flor, S.I.N. Heleno, H. E. Ferreira, & J.F.B.D. Fonseca (2012), Large Holocene Earthquakes in the Lower Tagus Valley Fault Zone, Central Portugal. *Seismol. Res. Lett.*, 83, 67-76.

Palano, M., González, P.J. , & Fernández, J. (2015), The diffuse plate boundary of Nubia and Iberia in the Western Mediterranean: crustal deformation evidence for viscous coupling and fragmented lithosphere. *Earth and Planetary Science Letters*, 430, 439-447, http://dx.doi.org/10.1016/j.epsl.2015.08.040.

Palano, M., Imprescia, P., Agnon, A. , & Gresta, S. (2018), An improved evaluation of the seismic/ geodetic deformation-rate ratio for the Zagros Fold-and-Thrust collisional belt. *Geophys. J. Int.*, 213, 194–209, doi: 10.1093/gji/ggx524

Payne, S., McCaffrey, R. , & King, R.W. (2008), Strain-rates and contemporary deformation in the Snake River Plain and surrounding Basin and Range from GPS and seismicity. *Geology*, 36(8), 647–650, doi: 10.1130/G25039A.1

Pereira, R. , & Alves, T.M. (2013), Crustal deformation and submarine canyon incision in a Meso-Cenozoic first-order transfer zone (SW Iberia, North Atlantic Ocean. *Tectonophysics*, 601, 148-162 DOI: 10.1016/j.tecto.2013.05.007

Petrie, E.J., King, M.A., Moore, P., & Lavallée, D.A. (2010), Higher-order

ionospheric effects on the GPS reference frameand velocities, *J. Geophys. Res. Solid Earth*, 115 (B03417), doi:10.1029/2009JB006677

Pinheiro, L., R. Wilson, R. Pena dos Reis, Whitmarsh, R., & A. Ribeiro (1996), The Western Iberian Margin: a geophysical and geological overview. In R. Whitmarsh, D. Daywer, A. Klaus, and D. Masson (Editors), Proceedings of the Ocean Drilling Program, Leg 149, Scientific Results Volume, IODP, Washington, 533–545.

Ramalho, M., Matias, L., Neres, M., Carafa, M.M.C, Carvalho, A. , & Costa, P. (2020), A sanity check for earthquake recurrence models used in PSHA of slow deforming regions: the case of SW Iberia. *Natural Hazards and Earth Systems Science Discussions*, https://doi.org/10.5194/nhess-2020-300

Rasmussen, E,S., Lomholt, S., Andersen, C. , & Vejbæk, O.V. (1988), Aspects of the structural evolution of the Lusitanian Basin in Portugal and the shelf and slope area offshore Portugal. *Tectonophysics*, 300, 199–225.

Reis, R., Pimentel, N., Fainstein, R., Reis, M, & Rasmussen, B. (2017), Influence of salt diapirism on the basin architecture and hydrocarbon prospects of the Western Iberian Margin. In Soto., J., Flinch, J. and Tari, G. (eds.), Permo-triassic Salt Provinces of Europe, North Africa and the Atlantic Margins, Elsevier, Amsterdam.

Ribeiro, A., Cabral, J., Baptista, R. , & Matias, L. (1996), Stress pattern in Portugal mainland and the adjacent Atlantic region, West Iberia. *Tectonics*, 15, 641–659

Shen, Z.-K.,Wang, M., Zeng, Y., &Wang, F. (2015), Optimal interpolation of spatially discretized geodetic data. *Bull. seism. Soc. Am.*, 105(4), 2117–2127.

Storchak, D.A., Harris, J., Brown, L. et al. (2020), Rebuild of the Bulletin of the International Seismological Centre (ISC)—part 2: 1980–2010. *Geosci. Lett.* 7, 18. https://doi.org/10.1186/s40562-020-00164-6

Stucchi, M., Rovida, A., Gómez, A., Alexandre, P., Camelbeeck, T., Demircioglu, M., Gasperini, P., Kouskouna, V., Musson, R., Radulian, M., Sesetyan, R., Vilanova, S., Baumont, D., Bungum, H., Fäh, D., Lenhardt, W., Makropoulos, K., Solares, J., Scotti, O. & Giardini, D. (2013), The SHARE European earthquake catalogue (SHEEC) 1000–1899. *Journal of Seismology*, 17. 523-544.

Sylvester, A. G. (1988), Strike-slip faults. *GSA Bulletin*, v. 100 (11), 1666-1703.

Vilanova, S.P., & J.F.B.D. Fonseca (2007), Probabilistic seismic-hazard assessment for Portugal. *Bull. Seismol. Soc. Am.,* 97, p. 1702–1717.

Walker, D. J. (1982), Final report: seismic interpretation for Petrogal concession areas 45, 46, 47/48. GPEP, Lisbon.

Wang, H., Wright, T. J., Liu-Zeng, J., & Peng, L. (2019), Strain-rate distribution in south-central Tibet from two decades of InSAR and GPS. *Geophysical Research Letters*, 46, https://doi.org/10.1029/2019GL081916

Wegmuller, U., Werner, C., Magnard, C., & Manconi, A. (2019), Co-seismic displacement vector retrieval for the Iran-Iraq Earthquake using Sentinel-1 (poster), ESA Living Planet Meeting Milano, Italy, 2019, https://www.gamma-rs.ch/uploads/media/2000-1_GAMMA_Software.pdf (last retrieved August 2, 2021).

Werner, C., Wegmuller, U., Strozzi, T., & Wiesman, A. (2000), GAMMA SAR and Interferometric software, ERS - ENVISAT Symposium, Gothenburg, Sweden, 16-20 Oct. 2000, https://www.gamma-rs.ch/uploads/media/2000-1_GAMMA_Software.pdf (last retrieved August 2, 2021).

Wessel, P., & Smith, W. H. F. (1991), Free software helps map and display data. *EOS Trans. AGU*, 72(41), 445–446. doi.org/10.1029/90EO00319.

Wilson, R.C.L., Hiscott, R.N., Willis, M.G., & Gradstein, P.M. (1989), The Lusitanian Basin of west-central Portugal: Mesozoic and Tertiary tectonic, stratigraphic and subsidence history. In Tankard, A.J., and Balkwill, H.R. (Eds.), Extensional Tectonics and Stratigraphy of the North Atlantic Margins. AAPG Mem. 46, 341-361.

Woessner, J., Laurentiu, D., Giardini, D., Crowley, H., Cotton, F., Grünthal, G., et al. (2015), The 2013 European seismic hazard model: key components and results. *Bull. Earthq. Eng.*, 13 (12), 3553–3596. doi:10.1007/s10518-015-9795-1.